

Robust 3D Shape Reconstruction in Zero-Shot from a Single Image in the Wild

Junhyeong Cho¹ Kim Youwang² Hunmin Yang^{1,4} Tae-Hyun Oh^{2,3,5}

¹ADD ²Department of EE, POSTECH ³Graduate School of AI, POSTECH ⁴KAIST

⁵Institute for Convergence Research and Education in Advanced Technology, Yonsei University

Abstract

Recent monocular 3D shape reconstruction methods have shown promising zero-shot results on object-segmented images without any occlusions. However, their effectiveness is significantly compromised in real-world conditions, due to imperfect object segmentation by off-the-shelf models and the prevalence of occlusions. To effectively address these issues, we propose a **unified regression model** that integrates segmentation and reconstruction, specifically designed for occlusion-aware 3D shape reconstruction. To facilitate its reconstruction in the wild, we also introduce a **scalable data synthesis pipeline** that simulates a wide range of variations in objects, occluders, and backgrounds. Training on our synthetic data enables the proposed model to achieve state-of-the-art zero-shot results on real-world images, using significantly fewer parameters than competing approaches.

1. Introduction

The abundance of large-scale 3D shapes [4, 7, 9, 10, 16, 33] has enabled the development of reconstruction models with strong generalization capabilities, even allowing for zero-shot monocular 3D shape reconstruction [25, 29, 41, 65, 67, 73]. However, all of these models are not deployable in real-world settings, as they assume object-centric images that have no backgrounds and occlusions. Thus, when applied to in-the-wild images, they depend on *off-the-shelf* segmentation models [32, 59]. This dependency introduces two main challenges: (i) accumulated errors from the off-the-shelf models, and (ii) the removal of occluded object parts during segmentation. Both challenges hinder the accurate reconstruction of 3D shapes, as shown in Figure 1.

To tackle these issues, we propose an occlusion-aware 3D shape reconstruction model (Fig. 2a) that jointly regresses the silhouettes of a salient object and its occluders, as well as camera intrinsics and a depth map to estimate the object’s visible 3D shape. Our model regresses its full 3D shape by utilizing the visible 3D shape and the silhouette of occluders. This approach enables the reconstruction of occluded object parts, making it particularly effective in



Figure 1. Single-view 3D shape reconstruction on real-world images [64]. Compared with LRM [25] that requires an off-the-shelf segmentation model (e.g., SAM [32]), our approach not only eliminates the need for such an additional model, but also achieves more robust reconstruction results, e.g., for occluded regions.

real-world conditions. However, a significant challenge remains: *how can we train our model for robust zero-shot reconstruction in the wild?* To achieve this goal, it is necessary to obtain large-scale diverse data that cover various real-world environments. However, the availability of real-world images annotated with precise 3D shapes is limited. An alternative approach is to synthesize realistic renderings from 3D object collections [4, 7, 9, 10, 16], but this is also limited by the availability of high-quality synthetic assets.

In this paper, we introduce a scalable data synthesis pipeline (Fig. 2b) that simulates a wide range of variations using generative models, thereby removing the reliance on limited real-world data or high-quality synthetic assets. Our pipeline first synthesizes foreground object images using a conditional generative model [83], with spatial conditions obtained by rendering 3D shapes available from extensive object collections [4, 9, 10]. Then, their backgrounds are generated by an object-aware background outpainting model [13]. For these synthesized images, we apply Copy-Paste augmentation [19] to simulate occluders on-the-fly during model training.

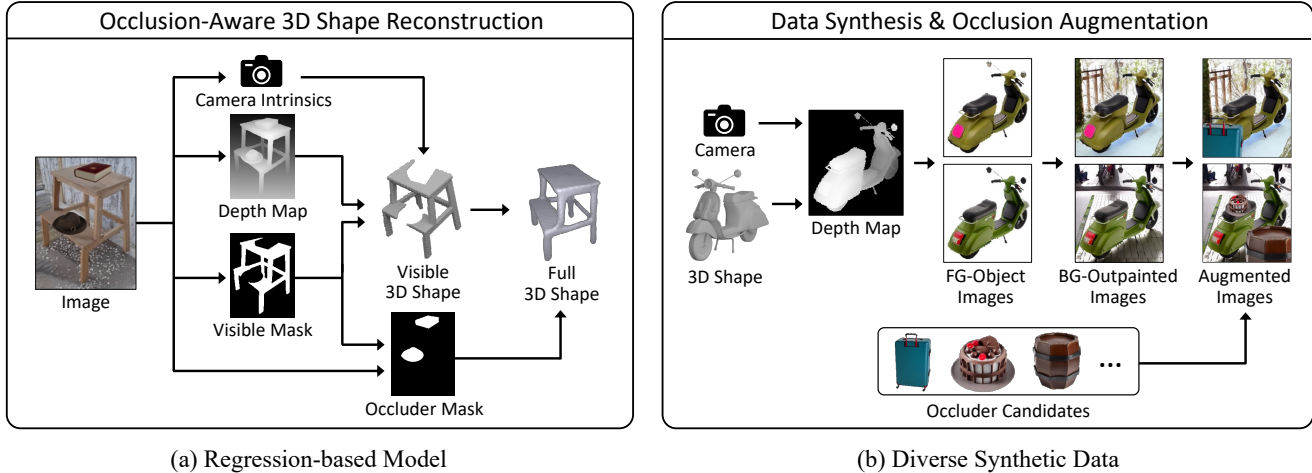


Figure 2. Proposed approach for zero-shot monocular 3D shape reconstruction in the wild. (a) Our model reconstructs the full 3D shape of a salient object using its visible 3D shape and the silhouette of its occluders. The visible 3D shape is estimated from camera intrinsics, depth map, and visible region of the object. (b) We create our training dataset by synthesizing diverse data. We render 3D shapes and then simulate their appearances and backgrounds using generative models. Occluders are dynamically inserted during model training.

By training the proposed model on our diverse synthetic data, we expose it to a wide variety of foreground objects, their occluders, and backgrounds. This process enables our model to focus on learning to capture domain-invariant and object-centric geometric priors. In this way, we improve its generalization across various environments.

To validate the effectiveness of our approach, we first create our training dataset by synthesizing diverse images using 3D shapes from Objaverse [10] and ShapeNet [4]. Then, we train our model on the data augmented with occlusions. We evaluate the model on the real-world benchmark, Pix3D [64], where it outperforms state-of-the-art models while using significantly fewer model parameters. In addition to the benchmark, we also qualitatively evaluate the proposed model on in-the-wild images from ObjectNet [2], OfficeHome [71], and PACS [35].

2. Related Work

Single-view 3D shape reconstruction in the wild. This task aims to estimate the 3D shape of an object from a single image captured in a real-world environment. It is challenging because objects exhibit a variety of 3D shapes while their appearances are greatly altered by environmental factors. To handle such variations, 3D shape reconstruction models [1, 6, 18, 20–23, 25, 28–30, 38, 41, 48, 50, 52, 65, 67, 69, 72, 73, 75–77, 79, 82, 85] should generalize well across various environments. However, the scarcity of real-world 3D data poses a significant obstacle in pursuing this goal. In this paper, we address this issue by synthesizing large-scale data using generative models.

Single-view 3D shape reconstruction methods fall into two categories: generative model-based approaches [41, 65, 73, 79] and regression model-based approaches [25, 29, 67].

The generative model-based approaches synthesize multi-view images using diffusion models like Zero-1-to-3 [39], which are effective to estimate 3D shapes with textures but incur significant computational costs. In contrast, the regression-based approaches estimate 3D shapes in a single forward pass, offering much greater efficiency.

Recent state-of-the-art methods in both approaches assume clean object-segmented images without occlusions, making them difficult to operate in real-world settings. In this work, we tackle this issue by introducing a unified regression model that both segments and reconstructs while accounting for occlusions. To the best of our knowledge, our work is the first regression-based approach for zero-shot single-view 3D shape reconstruction in the wild.

Improving model robustness to distribution shifts. It is common to exploit multiple domains for learning domain-invariant features [3, 12, 31, 34, 36, 44, 45, 62, 87, 88] to enhance the model robustness. However, multiple domains from real-world environments might not be accessible. To effectively tackle this issue, domain randomization methods [8, 14, 26, 46, 55, 60, 66, 68, 81] synthesize multiple domains via a random simulation of diverse scenarios. By exposing a model to randomized variations, it learns to capture generalizable representations capable of handling a wide range of variations encountered in real-world settings.

Following the paradigm of domain randomization, we simulate diverse variations in foreground objects, occluders, and backgrounds. However, this is not done completely randomly, as our background inpainting model [13] generates backgrounds while taking the objects into account. By training the proposed model on our synthesized data, it could learn to capture domain-invariant and object-centric geometric priors, useful for handling real-world objects.

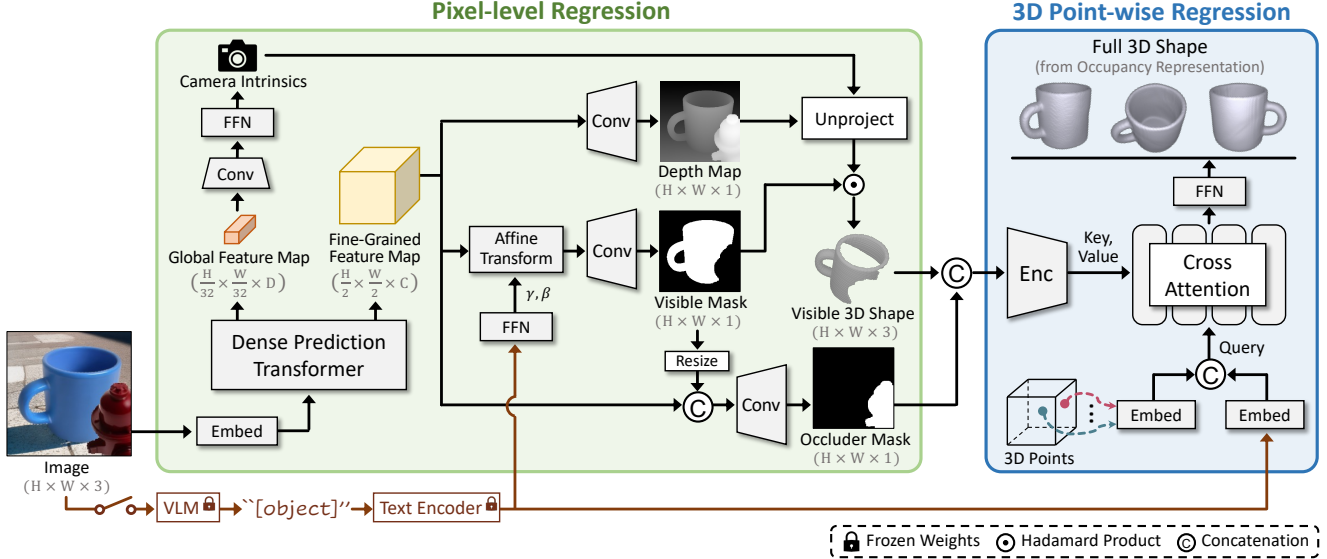


Figure 3. Overall architecture of the proposed model for occlusion-aware 3D shape reconstruction. Given an object-centric RGB image, our model leverages the backbone of Dense Prediction Transformer [58] to regress camera intrinsics, a depth map, a visible mask of a salient object, and an occluder mask that represents the object’s occluders. These components are used to derive the object’s visible 3D shape, which is then combined with the occluder mask to regress occupancy values of 3D point queries through cross-attention layers [70]. This process recovers the object’s full 3D shape, including occluded regions. To facilitate in-the-wild reconstruction, we optionally incorporate open-set category priors by estimating the object’s category, “[object]” (e.g., “cup”), using a vision-language model (VLM) [37].

Synthetic data generation. To train 3D shape reconstruction models, we can synthesize data by rendering 3D objects from extensive object collections [4, 7, 9, 10, 16, 33] via computer graphics tools. As long as sufficient 3D shape and texture assets are available for objects and environments, this approach could also facilitate 3D shape reconstruction in the wild. However, it is expensive to collect a great variety of high-quality assets (e.g., 4K-resolution texture maps, HDR environment maps) needed to bridge the gap between synthetic and real environments. Moreover, the diversity of object appearances and backgrounds depicted by rendered images is determined by the combination of available assets. Compared with these computer graphics tools, our data synthesis pipeline could simulate more diverse object appearances and backgrounds without relying on such additional high-quality assets, by leveraging generative models pre-trained on large-scale datasets.

Generative models with 3D assets. Recent works [17, 43, 84] use conditional generative models [49, 56, 83] to synthesize images with 3D assets for various tasks, e.g., object pose estimation. Compared with them, accurate preservation of silhouettes within spatial conditions is more crucial for 3D shape reconstruction. To better preserve silhouettes, our data synthesis pipeline employs a two-step generation process. We utilize initial guidance for foreground object synthesis and exploit a background outpainting model [13] specifically designed for preserving silhouettes. In this way, each synthesized image is paired with its precise 3D shape.



Figure 4. Effect of using an occluder mask. It enables full 3D shape reconstruction, even for occluded regions. Without identifying occluded regions, state-of-the-art methods [25, 29, 41, 65, 67, 73] struggle with occlusions, as they assume that the salient visible object in the current view is unobstructed.

3. Method

The proposed model (Fig. 3) aims to regress the full 3D shape of a salient object from a single image, including its visible and occluded regions (Fig. 4). Inspired by [29, 74], our model first regresses pixel-level information, which is used as condition to regress occupancy values of 3D point queries. These occupancy values represent the visible and hidden geometry of the salient object, while also accounting for occluded regions that were not addressed in [29, 74].

During pixel-level regression, our model regresses a depth map, a visible mask of the object, and an occluder mask that depicts the object’s occluders. It also estimates camera intrinsics to convert depth values into the object’s visible 3D shape in a viewer-centric coordinate system.

During 3D point-wise regression, our model regresses occupancy values of 3D point queries through cross-attention layers [70], utilizing features from the visible 3D shape and occluder mask as keys and values. This approach

can effectively reconstruct the object’s hidden geometry, with the help of learned 3D shape priors.

For in-the-wild images, identifying arbitrary salient objects is often challenging due to complex backgrounds or occlusions, which can result in noisy mask estimations. In this case, visible 3D shapes may mistakenly include background geometries. To address these issues, we optionally incorporate category-specific priors by leveraging a vision-language model [37] and CLIP text encoder [57]. Specifically, the vision-language model generates a **category-specific prompt** “[object]” (e.g., “cup” in Fig. 3) that describes the salient object in the input image. For stable inference with unseen object categories, we use an averaged CLIP text embedding obtained from the category-specific prompt and a **category-agnostic prompt** “object”. In cases where category priors are not used, our model relies solely on the category-agnostic prompt without estimating the object’s category.

3.1. Pixel-level Regression

For an object-centric RGB image $I \in \mathbb{R}^{H \times W \times 3}$, we first obtain image embeddings $\mathbf{E}_I \in \mathbb{R}^{(H/16) \times (W/16) \times D}$ using ResNet50 [24], as done in ViT-Hybrid [11]. Then, we feed the embeddings \mathbf{E}_I into the backbone of Dense Prediction Transformer (DPT) [58]. From the backbone, we extract a global feature map $\mathbf{X}_G \in \mathbb{R}^{(H/32) \times (W/32) \times D}$ and a fine-grained feature map $\mathbf{X}_F \in \mathbb{R}^{(H/2) \times (W/2) \times C}$. The global feature map \mathbf{X}_G is the reassembled output from the last transformer layer in DPT, while the fine-grained feature map \mathbf{X}_F is the output from the last fusion layer in DPT.

Camera intrinsics. To regress the visible 3D shape of the salient object, we estimate camera intrinsics $K \in \mathbb{R}^{3 \times 3}$ from the global feature map \mathbf{X}_G . Specifically, we obtain the camera intrinsics K by predicting a focal length scaling factor and principal point shifts, as done in [29]. The scaling factor adjusts a base focal length according to the image resolution $H \times W$, and the principal point shifts are also specified relative to the image resolution. These parameters are estimated from the global feature map \mathbf{X}_G using shallow convolutional layers, a pooling layer, and a feed forward network (FFN).

Depth map. To derive the visible 3D shape by unprojecting depth values using the estimated camera intrinsics K , we regress a depth map $\mathbf{M}_D \in \mathbb{R}^{H \times W \times 1}$ from the fine-grained feature map \mathbf{X}_F . For this regression, we use shallow convolutional layers with interpolation.

Visible mask. To identify the visible region of the salient object, we regress a visible mask $\mathbf{M}_V \in \mathbb{R}^{H \times W \times 1}$ from the fine-grained feature map \mathbf{X}_F . For precise regression, we adaptively adjust the fine-grained feature map \mathbf{X}_F based on the object’s category. Inspired by [25, 53, 54], we modulate the feature map using an affine transformation with a scaling factor $\gamma \in \mathbb{R}^C$ and a shift factor $\beta \in \mathbb{R}^C$, estimated

by an FFN with CLIP text encoder [57]. We modulate the feature map \mathbf{X}_F at each spatial location (i, j) as follows:

$$\bar{\mathbf{X}}_{F_{ij}} = (1 + \gamma) \mathbf{X}_{F_{ij}} + \beta, \quad (1)$$

where $\bar{\mathbf{X}}_F \in \mathbb{R}^{(H/2) \times (W/2) \times C}$. From this modulated feature map, we regress the visible mask \mathbf{M}_V using shallow convolutional layers with interpolation.

Visible 3D shape. Using the estimated camera intrinsics K , depth map \mathbf{M}_D , and visible mask \mathbf{M}_V , we derive the visible 3D shape $\mathbf{S}_V \in \mathbb{R}^{H \times W \times 3}$ that contains (x, y, z) -coordinates of each pixel location (i, j) as follows:

$$\mathbf{S}_{V_{ij}} = \mathbb{1}_{\{\mathbf{M}_{V_{ij}} \geq \eta\}} \cdot (\mathbf{M}_{D_{ij}} K^{-1} [i, j, 1]^\top), \quad (2)$$

where $\mathbb{1}_{\{\cdot\}}$ is an indicator function, and η denotes a threshold. We normalize \mathbf{S}_V to have a zero mean and a unit scale.

Occluder mask. To determine the object’s occluded region, we regress an occluder mask $\mathbf{M}_O \in \mathbb{R}^{H \times W \times 1}$ using the fine-grained feature map \mathbf{X}_F and visible mask \mathbf{M}_V . Specifically, we resize the visible mask to the resolution of $H/2 \times W/2$, and concatenate it with the feature map along the channel dimension. Then, we regress the occluder mask \mathbf{M}_O using shallow convolutional layers with interpolation.

3.2. 3D Point-wise Regression

We regress occupancy values of 3D point queries using cross-attention layers to effectively consider local features from pixel-level estimations; building on prior works [29, 74] and adding the ability to account for occluded regions. We begin by concatenating the visible 3D shape \mathbf{S}_V and the occluder mask \mathbf{M}_O along the channel dimension, which is then fed into an encoder. It produces Z -dimensional vectors that serve as keys and values in cross-attention layers.

For each 3D point query, we construct a Z -dimensional query vector by concatenating two $Z/2$ -dimensional embeddings: one from the point’s (x, y, z) -coordinates and the other from CLIP text encoder [57]. The query vectors are processed through L cross-attention layers, where each query independently attends to its relevant spatial features. Then, to reconstruct the object’s full 3D shape, we estimate the occupancy value of each query using an FFN.

3.3. Loss

We train our model using a binary cross-entropy loss for each regression of the visible mask \mathbf{M}_V , occluder mask \mathbf{M}_O , and occupancy values. For the regression of the depth map \mathbf{M}_D , we apply a scale- and shift-invariant MAE loss [15] over two regions: (i) the visible mask region using ground-truth depth, and (ii) the entire region using pseudo depth from a pre-trained depth estimator, referred to as auxiliary depth loss. For the regression of the camera intrinsics K , we use an MSE loss by comparing the visible 3D shape \mathbf{S}_V to the ground truth.

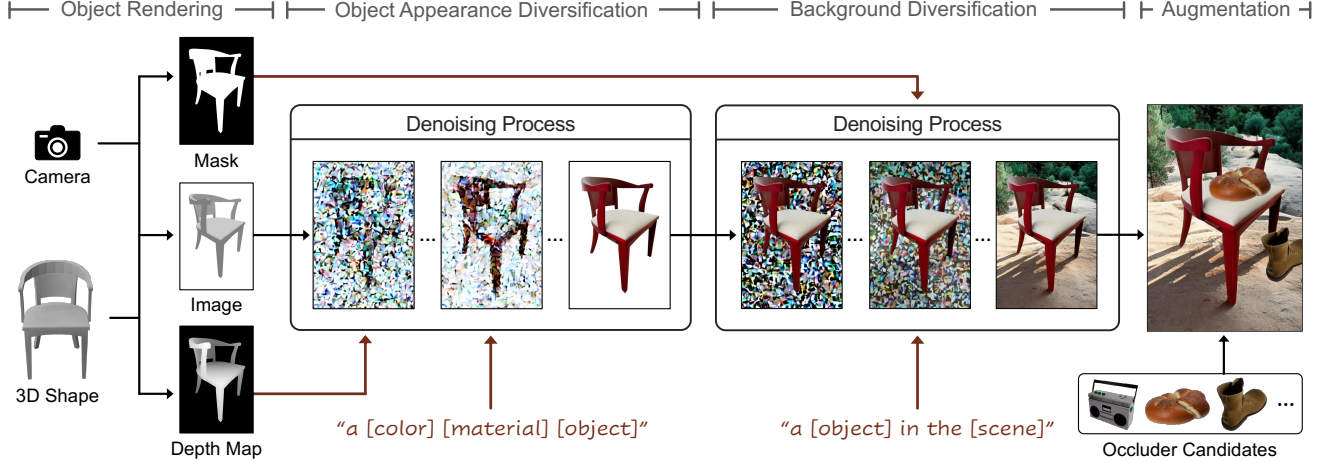


Figure 5. Overview of our data synthesis. Given a camera and 3D object, we render it to obtain an object mask, image, and depth map. We simulate object appearances via a conditional diffusion model [83] using the depth as its spatial condition and “a [color] [material] [object]” (e.g., “a red wood chair”) as its textual condition. To alleviate shape distortion by the generative model, we use the rendered image as initial guidance. We simulate its background via an object-aware background outpainting model [13] using the mask and “a [object] in the [scene]” (e.g., “a chair in the canyon”) as its textual condition. Then, we put occluders during data augmentation.

3.4. Implementation Details

We input an image of resolution $H \times W$, where $H = W = 224$. Using DPT-Hybrid [58], we extract the D -dimensional feature \mathbf{X}_G and C -dimensional feature \mathbf{X}_F , where $D = 768$ and $C = 256$. In eq. (2), we set $\eta = 0.5$. In L cross-attention layers, we employ Z -dimensional vectors, where $L = 2$ and $Z = 256$. During training, we use Depth Anything V2 [80] for auxiliary depth loss. At inference time, we optionally use LLaMA-VID [37] to identify the object’s category. Further details can be found in the supplementary material.

4. Data Synthesis

Our scalable data synthesis pipeline (Fig. 5) produces diverse images, along with their corresponding 3D shapes, camera parameters, depth maps, and masks. We use Copy-Paste [19] augmentation to dynamically insert occluders. Please see the supplementary material for more details.

4.1. Object Rendering

A great variety of 3D shapes can be readily obtained from 3D object collections [4, 7, 9, 10, 16, 33] or generative models [5, 40, 63, 76]. In line with ZeroShape [29], we utilize the same set of 3D objects spanning over 1,000 categories, including 52K objects from ShapeNetCore.v2 [4] and 42K objects from Objaverse-LVIS [10].

Each 3D object is rendered by multiple cameras constructed with varying camera distances, elevation angles, focal lengths, and LookAt points. This rendering process produces over 1 million object images, and each output is paired with precise 3D shapes, camera parameters, depth maps, and masks.

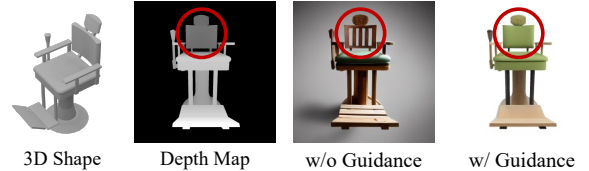


Figure 6. Effect of using initial guidance. The guidance assists in preserving the object silhouette depicted in the spatial condition.

4.2. Object Appearance Diversification

To simulate diverse visual variations in object appearances, we use ControlNet [83] which is a conditional diffusion model capable of realistically synthesizing diverse images. In our data synthesis, the generative model simulates a wide range of variations by using a depth map as its spatial condition and “a [color] [material] [object]” as its textual condition. Here, the placeholders [color] and [material] are replaced by words selected from pre-defined color and material lists, while [object] denotes the category of the used 3D object.

Initial guidance. The diffusion model [83] occasionally distorts the object silhouette depicted in the spatial condition. To alleviate this distortion, we utilize the rendered image as initial guidance. Motivated by SDEdit [47], we perturb the guidance with Gaussian noise and feed it to the model. Since the noisy guidance retains the original spatial structure, it effectively reduces silhouette distortion (Fig. 6).

4.3. Background Diversification

To simulate diverse backgrounds, we use an object-aware background outpainting model [13]. It adapts Stable Diffusion Inpainting 2.0 [61] by using modified ControlNet [83], allowing for background generation without extending the

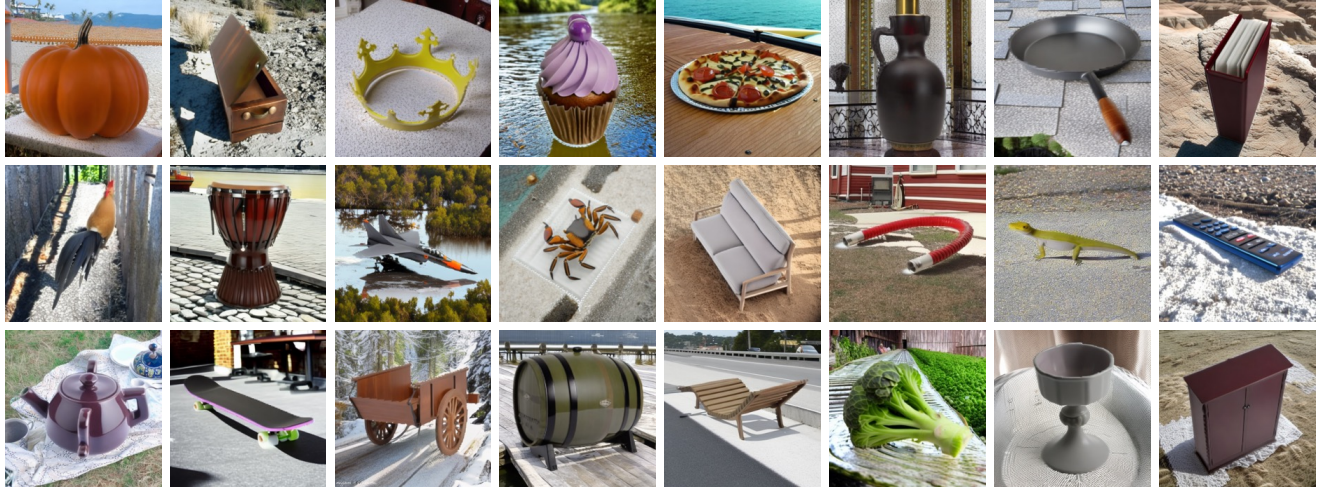


Figure 7. Diverse synthetic data produced by our scalable data synthesis pipeline. Based on 3D shape renderings from ShapeNetCore.v2 [4] and Objaverse-LVIS [10], we synthesize diverse images using ControlNet [83] and object-aware background outpainting model [13].

object’s silhouette. We generate various backgrounds using the object image, its mask, and the prompt “a [object] in the [scene]”, where [scene] is selected from scene categories [78, 86]. Ideally, it synthesizes backgrounds that appear to be captured by cameras with focal lengths similar to those used for the object’s rendering.

4.4. Augmentation

For images generated by our data synthesis (Fig. 7), we dynamically simulate occluders during model training through Copy-Paste augmentation [19] using our synthesized foreground objects. For stable estimation of camera intrinsics, we put objects rendered by similar focal lengths.

5. Experiments

5.1. Evaluation Settings

Protocol. To convert implicit 3D shape representation into explicit 3D meshes, we extract the isosurface from the implicit representation via the Marching Cubes [42] algorithm. Following [23, 50, 82], we align predicted and ground-truth meshes using the Iterative Closest Point algorithm. Then, we uniformly sample 10K points from each mesh.

Metrics. Using 10K sampled points, we compute Chamfer Distance (CD) and F-Score (FS) for quantitative evaluation, as in [27–29]. Specifically, $FS@{\tau}$ denotes the harmonic mean of $precision@{\tau}$ and $recall@{\tau}$, which represents the concordance between predicted and ground-truth points within a distance threshold τ .

Datasets. We evaluate our model on real-world object images from Pix3D [64], ObjectNet [2], OfficeHome [71], and PACS [35]. As Pix3D is the widely recognized benchmark for 3D shape reconstruction in the wild, we use it for comparison with other state-of-the-art models [25, 29].

5.2. Experimental Results

Quantitative comparison. Currently, there is no zero-shot monocular 3D shape reconstruction model capable of directly processing real-world images. Therefore, we compare our model with state-of-the-art reconstruction models, LRM [25] and ZeroShape [29], which operate on object-segmented images without occlusions. To ensure comprehensive comparisons with these strong baselines, we equip them with the off-the-shelf modal segmentation model, SAM [32], and amodal completion model, pix2gestalt [51].

In Table 1, we evaluate the baselines and our model on the Pix3D benchmark [64]. Although the proposed model does not utilize such off-the-shelf models, it significantly outperforms them. In terms of $FS@{\tau}$, our model outperforms the strongest baseline ZeroShape_{w/SAM + pix2gestalt} by a large margin of 16.4% (39.1 vs. 33.6). When it comes to CD, the proposed model also substantially surpasses the strongest baseline by a large margin of 15.8% (0.095 vs. 0.110); lower is better for CD.

Compared with the baselines, the proposed model requires significantly fewer model parameters, as it jointly regresses pixel-level information (depth map, visible mask, occluder mask) using the shared feature map X_F . For example, the number of learnable parameters used by our model is less than 1/12 of the parameters used by LRM_{w/SAM + pix2gestalt}, as shown in Table 1.

Zero-shot capability of our model. In Table 1, the results obtained by ours using the category-agnostic prompt “object” demonstrate the zero-shot capability of the proposed model, which does not assume any object categories. It still substantially outperforms the strongest baseline, ZeroShape_{w/SAM + pix2gestalt}, e.g., 13.7% (38.2 vs. 33.6) with regard to $FS@{\tau}$.

Model	Off-the-shelf Model		#Params	Pix3D Evaluation				CD \downarrow
	Modal Segmentation	Amodal Completion		FS@ $\tau \uparrow$	FS@ $2\tau \uparrow$	FS@ $3\tau \uparrow$	FS@ $5\tau \uparrow$	
LRM [25]	SAM [32]	—	> 1100M	31.0	54.5	69.9	87.1	0.121
	SAM [32]	pix2gestalt [51]		> 2400M	31.1	54.9	70.6	87.7
ZeroShape [29]	SAM [32]	—	> 800M	32.1	56.8	72.1	88.0	0.116
	SAM [32]	pix2gestalt [51]		> 2100M	33.6	59.0	74.2	89.2
Ours (category-agnostic)	—	—	193.7M	38.2	65.3	79.9	92.5	0.097
Ours (category-specific)	—	—	193.7M + α	39.1	66.2	80.4	92.6	0.095

Table 1. Quantitative comparison of single-view 3D shape reconstruction results on the real-world benchmark, Pix3D [64]. We compare our model with state-of-the-art models, LRM [25] and ZeroShape [29]. As these models assume object-segmented images without any occlusions, they require an off-the-shelf modal segmentation model (*e.g.*, SAM [32]). For occlusion-aware 3D shape reconstruction, they need an additional amodal completion model (*e.g.*, pix2gestalt [51]). Our approach not only eliminates the need for such off-the-shelf models but also substantially outperforms those competing approaches. In the *Overhead* column, α denotes the number of parameters used by a vision-language model (VLM) [37], which is optionally used for leveraging category-specific priors.

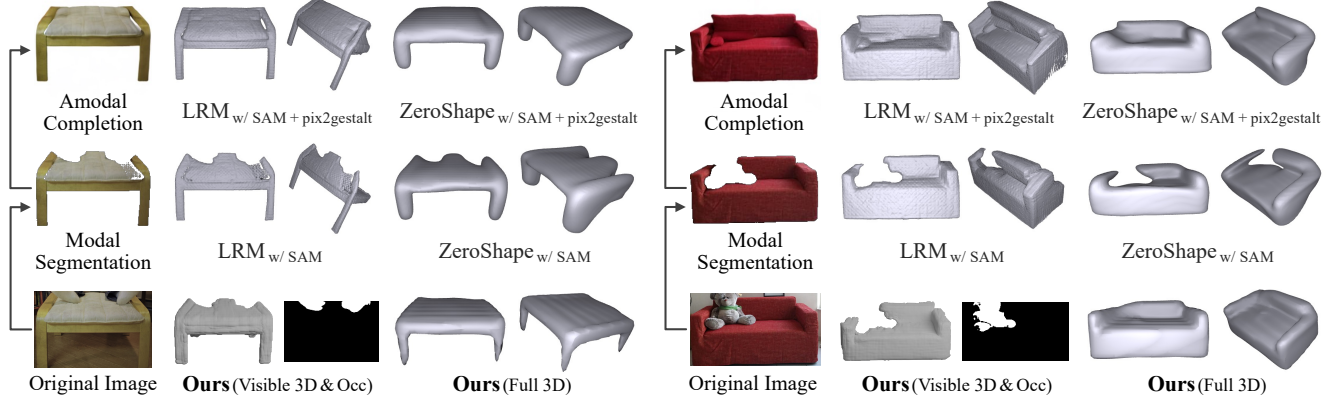


Figure 8. Qualitative comparison of single-view 3D shape reconstruction results on the real-world benchmark, Pix3D [64]. We compare our model with state-of-the-art models, LRM [25] and ZeroShape [29], which take modal segmentation outputs (from SAM [32]) or amodal completion outputs (from pix2gestalt [51]) as inputs. In contrast, the proposed model directly takes original images as inputs, and performs occlusion-aware 3D shape reconstruction by considering regressed visible 3D shapes and identified occluded regions.

Qualitative comparison. Figure 8 presents single-view 3D shape reconstruction results on real-world images from Pix3D [64]. Unlike our model that directly takes original input images, LRM [25] and ZeroShape [29] require object-segmented images as inputs. When these models utilize an off-the-shelf modal segmentation model (*e.g.*, SAM [32]), they struggle to estimate the geometry for occluded regions. For occlusion-aware reconstruction, they must incorporate an additional amodal completion model (*e.g.*, pix2gestalt [51]), but this approach often leads to error accumulation from segmentation and amodal completion processes. Even with well-completed amodal images, reconstruction errors persist (see $LRM_{w/SAM + pix2gestalt}$ in the left column). This might be due to the compatibility issues between the images synthesized by pix2gestalt and LRM, as these models were trained on different datasets. In contrast, our model achieves promising results without the need to heavily pre-process input images through the off-the-shelf segmentation or amodal completion models.

Reconstruction of diverse objects. Figure 9 presents single-view 3D shape reconstruction results on real-world images from ObjectNet [2], OfficeHome [71], and PACS [35]. By leveraging learned priors, the proposed model can regress 3D shapes of various objects captured in real-world environments.

5.3. More Analyses

Effects of VLM. In Table 2, we examine the effects of category-specific priors using the VLM, LLaMA-VID [37]. The evaluation results are competitive when compared to using ground-truth object categories, which demonstrates that our model can effectively utilize category-specific priors at inference time, with the help of the VLM.

Effects of auxiliary depth loss. As described in Section 3, we utilize Depth Anything V2 [80] to estimate depth values for the entire image region, because our data synthesis pipeline only provides depth values for object areas, *i.e.*, excluding occluders and backgrounds. Without the auxiliary



Figure 9. Single-view 3D shape reconstruction of diverse object shapes. We qualitatively evaluate our model on real-world object images from ObjectNet [2], OfficeHome [71], and PACS [35]. The proposed model achieves promising in-the-wild reconstruction results, which demonstrates that our regression-based model has effectively learned generalizable 3D shape priors.

Category-Specific Prompt	Pix3D Evaluation		
	FS@ $\tau \uparrow$	FS@ $5\tau \uparrow$	CD \downarrow
Estimated from VLM [37]	39.1	92.6	0.095
Ground Truth	39.6	92.8	0.094

Table 2. Effects of using a VLM (LLaMA-VID [37]) for leveraging category-specific priors. On Pix3D [64], we compare it with the result obtained from using ground-truth object categories.

depth loss, we observed that predicted depth values for non-object regions are quite inaccurate, leading to worse results as shown in Table 3. This loss aids in accurately regressing depth values for the entire image, which helps to distinguish the salient object from its occluders and backgrounds based on depth values. In addition, the auxiliary loss prevents our model from overfitting to our synthesized data.

Effects of occluders. To evaluate the contribution of occlusion-aware 3D shape reconstruction, we remove the occluder mask estimation branch while not augmenting our synthesized data with occluders. Although this approach fairly estimates visible 3D shapes, it struggles to reconstruct full 3D shapes when the salient object is occluded. As a result, its performance is degraded as shown in Table 3.

Effects of text prompts. We utilize category prompts to incorporate semantic priors into our model. When we do not use any text prompts, our model sometimes mistakenly separates a single object into a visible region and an occluder region based on depth values. Moreover, without the priors, our model struggles when the visible 3D shape is noisy (*e.g.*, including background geometry), as it becomes difficult to distinguish the object from the background solely using the 3D geometry, without additional visual cues. Consequently, its accuracy is diminished as shown in Table 3. Please refer to the supplementary material for more details.

Model	Pix3D Evaluation		
	FS@ $\tau \uparrow$	FS@ $5\tau \uparrow$	CD \downarrow
Ours <i>w/o auxiliary depth</i>	35.9	90.7	0.105
Ours <i>w/o occluders</i>	37.7	91.2	0.102
Ours <i>w/o text prompt</i>	38.0	91.5	0.101
Ours	39.6	92.8	0.094

Table 3. Effects of each key component. On Pix3D [64], we analyze the accuracy of our model by ablating components. In these experiments, we use ground-truth object categories.

6. Limitations

While our model can reconstruct full 3D shapes (including occluded regions), it may struggle to estimate 3D shapes for object parts clipped by image boundaries. As in other state-of-the-art methods [25, 29, 41, 65, 67, 73], our model still assumes the entire shape of the salient object from the current view is captured in the image (except occlusions).

Using depth and category priors, our model can fairly distinguish the salient object from its occluders. However, inherent ambiguity in the training dataset may still cause errors. For example, some “bed” 3D objects consist only of bed frames, while others include pillows on the frames.

7. Conclusion

To enable zero-shot single-view reconstruction in the wild, we presented (i) a unified regression model for occlusion-aware 3D shape reconstruction, and (ii) a scalable data synthesis pipeline for creating our training dataset. Our approach achieved state-of-the-art performance on in-the-wild images. Unlike other competing methods, our model does not use off-the-shelf segmentation or amodal completion models, leading to significantly fewer model parameters.

Acknowledgments. This work was supported by ADD grant funded by the Korean government. T.-H. Oh and K. Youwang were partially supported by IITP grant funded by the Korean government (MSIT) (No.2020-0-00004 (7%), Development of Previsional Intelligence based on Long-term Visual Memory Network; No.RS-2021-II212068 (7%), Artificial Intelligence Innovation Hub; No.RS-2022-II220290 (7%), Visual Intelligence for Space-Time Understanding and Generation based on Multi-layered Visual Common Sense).

References

- [1] Kalyan Vasudev Alwala, Abhinav Gupta, and Shubham Tulsiani. Pre-train, Self-train, Distill: A simple recipe for Super-sizing 3D Reconstruction. In *Proceedings of the IEEE/CVF Conference on Computer Vision and Pattern Recognition (CVPR)*, 2022. [2](#)
- [2] Andrei Barbu, David Mayo, Julian Alverio, William Luo, Christopher Wang, Dan Gutfreund, Josh Tenenbaum, and Boris Katz. Objectnet: A large-scale bias-controlled dataset for pushing the limits of object recognition models. In *Advances in Neural Information Processing Systems (NeurIPS)*, 2019. [2, 6, 7, 8](#)
- [3] Fabio Maria Carlucci, Antonio D’Innocente, Silvia Bucci, Barbara Caputo, and Tatiana Tommasi. Domain Generalization by Solving Jigsaw Puzzles. In *Proceedings of the IEEE/CVF Conference on Computer Vision and Pattern Recognition (CVPR)*, 2019. [2](#)
- [4] Angel X. Chang, Thomas Funkhouser, Leonidas Guibas, Pat Hanrahan, Qixing Huang, Zimo Li, Silvio Savarese, Manolis Savva, Shuran Song, Hao Su, Jianxiong Xiao, Li Yi, and Fisher Yu. ShapeNet: An Information-Rich 3D Model Repository. *arXiv preprint arXiv:1512.03012*, 2015. [1, 2, 3, 5, 6](#)
- [5] Gene Chou, Yuval Bahat, and Felix Heide. Diffusion-SDF: Conditional Generative Modeling of Signed Distance Functions. In *Proceedings of the IEEE/CVF International Conference on Computer Vision (ICCV)*, 2023. [5](#)
- [6] Christopher B. Choy, Danfei Xu, JunYoung Gwak, Kevin Chen, and Silvio Savarese. 3D-R2N2: A Unified Approach for Single and Multi-view 3D Object Reconstruction. In *Proceedings of the European Conference on Computer Vision (ECCV)*, 2016. [2](#)
- [7] Jasmine Collins, Shubham Goel, Kenan Deng, Achleshwar Luthra, Leon Xu, Erhan Gundogdu, Xi Zhang, Tomas F. Yago Vicente, Thomas Dideriksen, Himanshu Arora, Matthieu Guillaumin, and Jitendra Malik. ABO: Dataset and Benchmarks for Real-World 3D Object Understanding. In *Proceedings of the IEEE/CVF Conference on Computer Vision and Pattern Recognition (CVPR)*, 2022. [1, 3, 5](#)
- [8] Atabak Dehban, João Borrego, Rui Figueiredo, Plinio Moreno, Alexandre Bernardino, and Josá Santos-Victor. The impact of domain randomization on object detection: A case study on parametric shapes and synthetic textures. In *IEEE/RSJ International Conference on Intelligent Robots and Systems (IROS)*, 2019. [2](#)
- [9] Matt Deitke, Ruoshi Liu, Matthew Wallingford, Huong Ngo, Oscar Michel, Aditya Kusupati, Alan Fan, Christian Laforte, Vikram Voleti, Samir Yitzhak Gadre, Eli VanderBilt, Aniruddha Kembhavi, Carl Vondrick, Georgia Gkioxari, Kiana Ehsani, Ludwig Schmidt, and Ali Farhadi. Objaverse-XL: A Universe of 10M+ 3D Objects. In *Advances in Neural Information Processing Systems (NeurIPS)*, 2023. [1, 3, 5](#)
- [10] Matt Deitke, Dustin Schwenk, Jordi Salvador, Luca Weihs, Oscar Michel, Eli VanderBilt, Ludwig Schmidt, Kiana Ehsani, Aniruddha Kembhavi, and Ali Farhadi. Objaverse: A Universe of Annotated 3D Objects. In *Proceedings of the IEEE/CVF Conference on Computer Vision and Pattern Recognition (CVPR)*, 2023. [1, 2, 3, 5, 6](#)
- [11] Alexey Dosovitskiy, Lucas Beyer, Alexander Kolesnikov, Dirk Weissenborn, Xiaohua Zhai, Thomas Unterthiner, Mostafa Dehghani, Matthias Minderer, Georg Heigold, Sylvain Gelly, Jakob Uszkoreit, and Neil Houlsby. An Image is Worth 16x16 Words: Transformers for Image Recognition at Scale. In *International Conference on Learning Representations (ICLR)*, 2021. [4](#)
- [12] Qi Dou, Daniel C. Castro, Konstantinos Kamnitsas, and Ben Glocker. Domain Generalization via Model-Agnostic Learning of Semantic Features. In *Advances in Neural Information Processing Systems (NeurIPS)*, 2019. [2](#)
- [13] Amir Erfan Eshratifar, Joao V. B. Soares, Kapil Thadani, Shaunak Mishra, Mikhail Kuznetsov, Yueh-Ning Ku, and Paloma de Juan. Salient Object-Aware Background Generation using Text-Guided Diffusion Models. In *Proceedings of the IEEE/CVF Conference on Computer Vision and Pattern Recognition (CVPR) Workshops*, 2024. [1, 2, 3, 5, 6](#)
- [14] Ioannis Exarchos, Yifeng Jiang, Wenhao Yu, and C. Karen Liu. Policy Transfer via Kinematic Domain Randomization and Adaptation. In *International Conference on Robotics and Automation (ICRA)*, 2021. [2](#)
- [15] Towards Robust Monocular Depth Estimation: Mixing Datasets for Zero-shot Cross-dataset Transfer. René Ranftl and Katrin Lasinger and David Hafner and Konrad Schindler and Vladlen Koltun. *IEEE Transactions on Pattern Analysis and Machine Intelligence (TPAMI)*, 2020. [4](#)
- [16] Huan Fu, Rongfei Jia, Lin Gao, Mingming Gong, Binqiang Zhao, Steve Maybank, and Dacheng Tao. 3D-FUTURE: 3D Furniture shape with TextURE. In *International Journal of Computer Vision (IJCV)*, 2021. [1, 3, 5](#)
- [17] Yongtao Ge, Wenjia Wang, Yongfan Chen, Hao Chen, and Chunhua Shen. 3D Human Reconstruction in the Wild with Synthetic Data Using Generative Models. *arXiv preprint arXiv:2403.11111*, 2024. [3](#)
- [18] Kyle Genova, Forrester Cole, Avneesh Sud, Aaron Sarna, and Thomas Funkhouser. Local Deep Implicit Functions for 3D Shape. In *Proceedings of the IEEE/CVF Conference on Computer Vision and Pattern Recognition (CVPR)*, 2020. [2](#)
- [19] Golnaz Ghiasi, Yin Cui, Aravind Srinivas, Rui Qian, Tsung-Yi Lin, Ekin D. Cubuk, Quoc V. Le, and Barret Zoph. Simple Copy-Paste is a Strong Data Augmentation Method for Instance Segmentation. In *Proceedings of the IEEE/CVF Conference on Computer Vision and Pattern Recognition (CVPR)*, 2021. [1, 5, 6](#)

[20] Rohit Girdhar, David F. Fouhey, Mikel Rodriguez, and Abhinav Gupta. Learning a Predictable and Generative Vector Representation for Objects. In *Proceedings of the European Conference on Computer Vision (ECCV)*, 2016. 2

[21] Georgia Gkioxari, Jitendra Malik, and Justin Johnson. Mesh R-CNN. In *Proceedings of the IEEE/CVF International Conference on Computer Vision (ICCV)*, 2019.

[22] Shubham Goel, Angjoo Kanazawa, and Jitendra Malik. Shape and Viewpoint without Keypoints. In *Proceedings of the European Conference on Computer Vision (ECCV)*, 2020.

[23] Thibault Groueix, Matthew Fisher, Vladimir G. Kim, Bryan C. Russell, and Mathieu Aubry. AtlasNet: A Papier-Mâché Approach to Learning 3D Surface Generation. In *Proceedings of the IEEE Conference on Computer Vision and Pattern Recognition (CVPR)*, 2018. 2, 6

[24] He, Kaiming and Zhang, Xiangyu and Ren, Shaoqing and Sun, Jian. Deep Residual Learning for Image Recognition. In *Proceedings of the IEEE Conference on Computer Vision and Pattern Recognition (CVPR)*, pages 770–778, 2016. 4

[25] Yicong Hong, Kai Zhang, Jiuxiang Gu, Sai Bi, Yang Zhou, Difan Liu, Feng Liu, Kalyan Sunkavalli, Trung Bui, and Hao Tan. LRM: Large Reconstruction Model for Single Image to 3D. In *International Conference on Learning Representations (ICLR)*, 2024. 1, 2, 3, 4, 6, 7, 8

[26] Jiaxing Huang, Dayan Guan, Aoran Xiao, and Shijian Lu. FSDR: Frequency Space Domain Randomization for Domain Generalization. In *Proceedings of the IEEE/CVF Conference on Computer Vision and Pattern Recognition (CVPR)*, 2021. 2

[27] Zixuan Huang, Stefan Stojanov, Anh Thai, Varun Jampani, and James M. Rehg. Planes vs. Chairs: Category-guided 3D shape learning without any 3D cues. In *Proceedings of the European Conference on Computer Vision (ECCV)*, 2022. 6

[28] Zixuan Huang, Varun Jampani, Anh Thai, Yuanzhen Li, Stefan Stojanov, and James M. Rehg. ShapeClipper: Scalable 3D Shape Learning from Single-View Images via Geometric and CLIP-based Consistency. In *Proceedings of the IEEE/CVF Conference on Computer Vision and Pattern Recognition (CVPR)*, 2023. 2

[29] Zixuan Huang, Stefan Stojanov, Anh Thai, Varun Jampani, and James M. Rehg. ZeroShape: Regression-based Zero-shot Shape Reconstruction. In *Proceedings of the IEEE/CVF Conference on Computer Vision and Pattern Recognition (CVPR)*, 2024. 1, 2, 3, 4, 5, 6, 7, 8

[30] Angjoo Kanazawa, Shubham Tulsiani, Alexei A. Efros, and Jitendra Malik. Learning Category-Specific Mesh Reconstruction from Image Collections. In *Proceedings of the European Conference on Computer Vision (ECCV)*, 2018. 2

[31] Donghyun Kim, Kuniaki Saito, Tae-Hyun Oh, Bryan A. Plummer, Stan Sclaroff, and Kate Saenko. Cross-domain Self-supervised Learning for Domain Adaptation with Few Source Labels. In *Proceedings of the IEEE/CVF International Conference on Computer Vision (ICCV)*, 2021. 2

[32] Alexander Kirillov, Eric Mintun, Nikhila Ravi, Hanzi Mao, Chloe Rolland, Laura Gustafson, Tete Xiao, Spencer Whitehead, Alexander C. Berg, Wan-Yen Lo, Piotr Dollár, and Ross Girshick. Segment Anything. In *Proceedings of the IEEE/CVF International Conference on Computer Vision (ICCV)*, 2023. 1, 6, 7

[33] Sebastian Koch, Albert Matveev, Zhongshi Jiang, Francis Williams, Alexey Artemov, Evgeny Burnaev, Marc Alexa, Denis Zorin, and Daniele Panozzo. ABC: A Big CAD Model Dataset For Geometric Deep Learning. In *Proceedings of the IEEE/CVF Conference on Computer Vision and Pattern Recognition (CVPR)*, 2019. 1, 3, 5

[34] Pang Wei Koh, Shiori Sagawa, Henrik Marklund, Sang Michael Xie, Marvin Zhang, Akshay Balsubramani, Weihua Hu, Michihiro Yasunaga, Richard Lanas Phillips, Irena Gao, Tony Lee, Etienne David, Ian Stavness, Wei Guo, Berton A. Earnshaw, Imran S. Haque, Sara Beery, Jure Leskovec, Anshul Kundaje, Emma Pierson, Sergey Levine, Chelsea Finn, and Percy Liang. WILDS: A Benchmark of in-the-Wild Distribution Shifts. In *International Conference on Machine Learning (ICML)*, 2021. 2

[35] Da Li, Yongxin Yang, Yi-Zhe Song, and Timothy M. Hospedales. Deeper, Broader and Artier Domain Generalization. In *Proceedings of the IEEE International Conference on Computer Vision (ICCV)*, 2017. 2, 6, 7, 8

[36] Da Li, Jianshu Zhang, Yongxin Yang, Cong Liu, Yi-Zhe Song, and Timothy M. Hospedales. Episodic Training for Domain Generalization. In *Proceedings of the IEEE/CVF International Conference on Computer Vision (ICCV)*, 2019. 2

[37] Yanwei Li, Chengyao Wang, and Jiaya Jia. LLaMA-VID: An Image is Worth 2 Tokens in Large Language Models. In *Proceedings of the European Conference on Computer Vision (ECCV)*, 2024. 3, 4, 5, 7, 8

[38] Haolin Liu, Yujian Zheng, Guanying Chen, Shuguang Cui, and Xiaoguang Han. Towards High-Fidelity Single-view Holistic Reconstruction of Indoor Scenes. In *Proceedings of the European Conference on Computer Vision (ECCV)*, 2022. 2

[39] Ruoshi Liu, Rundi Wu, Basile Van Hoorick, Pavel Tokmakov, Sergey Zakharov, and Carl Vondrick. Zero-1-to-3: Zero-shot One Image to 3D Object. In *Proceedings of the IEEE/CVF International Conference on Computer Vision (ICCV)*, 2023. 2

[40] Zhen Liu, Yao Feng, Michael J. Black, Derek Nowrouzezahrai, Liam Paull, and Weiyang Liu. MeshDiffusion: Score-based Generative 3D Mesh Modeling. In *International Conference on Learning Representations (ICLR)*, 2023. 5

[41] Xiaoxiao Long, Yuan-Chen Guo, Cheng Lin, Yuan Liu, Zhiyang Dou, Lingjie Liu, Yuexin Ma, Song-Hai Zhang, Marc Habermann, Christian Theobalt, and Wenping Wang. Wonder3D: Single Image to 3D using Cross-Domain Diffusion. In *Proceedings of the IEEE/CVF Conference on Computer Vision and Pattern Recognition (CVPR)*, 2024. 1, 2, 3, 8

[42] William E. Lorensen and Harvey E. Cline. Marching cubes: A high resolution 3D surface construction algorithm. *ACM SIGGRAPH Computer Graphics*, 21(4), 1987. 6

[43] Wufei Ma, Qihao Liu, Jiahao Wang, Angtian Wang, Xiaodong Yuan, Yi Zhang, Zihao Xiao, Guofeng Zhang, Beijia Lu,

Ruxiao Duan, Yongrui Qi, Adam Kortylewski, Yaoyao Liu, and Alan Yuille. Generating Images with 3D Annotations Using Diffusion Models. In *International Conference on Learning Representations (ICLR)*, 2024. 3

[44] Divyat Mahajan, Shruti Tople, and Amit Sharma. Domain Generalization using Causal Matching. In *International Conference on Machine Learning (ICML)*, 2021. 2

[45] Toshihiko Matsuura and Tatsuya Harada. Domain Generalization Using a Mixture of Multiple Latent Domains. In *Proceedings of the AAAI Conference on Artificial Intelligence (AAAI)*, 2020. 2

[46] Bhairav Mehta, Manfred Diaz, Florian Golemo, Christopher J. Pal, and Liam Paull. Active Domain Randomization. In *Conference on Robot Learning (CoRL)*, 2019. 2

[47] Chenlin Meng, Yutong He, Yang Song, Jiaming Song, Jiajun Wu, Jun-Yan Zhu, and Stefano Ermon. SDEdit: Guided Image Synthesis and Editing with Stochastic Differential Equations. In *International Conference on Learning Representations (ICLR)*, 2022. 5

[48] Lars Mescheder, Michael Oechsle, Michael Niemeyer, Sebastian Nowozin, and Andreas Geiger. Occupancy Networks: Learning 3D Reconstruction in Function Space. In *Proceedings of the IEEE/CVF Conference on Computer Vision and Pattern Recognition (CVPR)*, 2019. 2

[49] Chong Mou, Xintao Wang, Liangbin Xie, Yanze Wu, Jian Zhang, Zhongang Qi, Ying Shan, and Xiaohu Qie. T2I-Adapter: Learning Adapters to Dig out More Controllable Ability for Text-to-Image Diffusion Models. *arXiv preprint arXiv:2302.08453*, 2023. 3

[50] Yinyu Nie, Xiaoguang Han, Shihui Guo, Yujian Zheng, Jian Chang, and Jian Jun Zhang. Total3DUnderstanding: Joint Layout, Object Pose and Mesh Reconstruction for Indoor Scenes from a Single Image. In *Proceedings of the IEEE/CVF Conference on Computer Vision and Pattern Recognition (CVPR)*, 2020. 2, 6

[51] Ege Ozguroglu, Ruoshi Liu, Dídac Surís, Dian Chen, Achal Dave, Pavel Tokmakov, and Carl Vondrick. pix2gestalt: Amodal Segmentation by Synthesizing Wholes. In *Proceedings of the IEEE/CVF Conference on Computer Vision and Pattern Recognition (CVPR)*, 2024. 6, 7

[52] Junyi Pan, Xiaoguang Han, Weikai Chen, Jiapeng Tang, and Kui Jia. Deep Mesh Reconstruction from Single RGB Images via Topology Modification Networks. In *Proceedings of the IEEE/CVF International Conference on Computer Vision (ICCV)*, 2019. 2

[53] William Peebles and Saining Xie. Scalable Diffusion Models with Transformers. In *Proceedings of the IEEE/CVF International Conference on Computer Vision (ICCV)*, 2023. 4

[54] Ethan Perez, Florian Strub, Harm de Vries, Vincent Dumoulin, and Aaron Courville. FiLM: Visual Reasoning with a General Conditioning Layer. In *Proceedings of the AAAI Conference on Artificial Intelligence (AAAI)*, 2018. 4

[55] Ayush Prakash, Shaad Boochoon, Mark Brophy, David Acuna, Eric Cameracci, Gavriel State, Omer Shapira, and Stan Birchfield. Structured Domain Randomization: Bridging the Reality Gap by Context-Aware Synthetic Data. In *International Conference on Robotics and Automation (ICRA)*, 2019. 2

[56] Can Qin, Shu Zhang, Ning Yu, Yihao Feng, Xinyi Yang, Yingbo Zhou, Huan Wang, Juan Carlos Niebles, Caiming Xiong, Silvio Savarese, Stefano Ermon, Yun Fu, and Ran Xu. UniControl: A Unified Diffusion Model for Controllable Visual Generation In the Wild. In *Advances in Neural Information Processing Systems (NeurIPS)*, 2023. 3

[57] Alec Radford, Jong Wook Kim, Chris Hallacy, Aditya Ramesh, Gabriel Goh, Sandhini Agarwal, Girish Sastry, Amanda Askell, Pamela Mishkin, Jack Clark, Gretchen Krueger, and Ilya Sutskever. Learning Transferable Visual Models From Natural Language Supervision. In *International Conference on Machine Learning (ICML)*, 2021. 4

[58] René Ranftl, Alexey Bochkovskiy, and Vladlen Koltun. Vision Transformers for Dense Prediction. In *Proceedings of the IEEE/CVF International Conference on Computer Vision (ICCV)*, 2021. 3, 4, 5

[59] Nikhila Ravi, Valentin Gabeur, Yuan-Ting Hu, Ronghang Hu, Chaitanya Ryali, Tengyu Ma, Haitham Khedr, Roman Rädle, Chloe Rolland, Laura Gustafson, Eric Mintun, Junting Pan, Kalyan Vasudev Alwala, Nicolas Carion, Chao-Yuan Wu, Ross Girshick, Piotr Dollár, and Christoph Feichtenhofer. SAM 2: Segment Anything in Images and Videos. *arXiv preprint arXiv:2408.00714*, 2024. 1

[60] Xinyi Ren, Jianlan Luo, Eugen Solowjow, Juan Aparicio Ojea, Abhishek Gupta, Aviv Tamar, and Pieter Abbeel. Domain Randomization for Active Pose Estimation. In *International Conference on Robotics and Automation (ICRA)*, 2019. 2

[61] Robin Rombach, Andreas Blattmann, Dominik Lorenz, Patrick Esser, and Björn Ommer. High-Resolution Image Synthesis with Latent Diffusion Models. In *Proceedings of the IEEE/CVF Conference on Computer Vision and Pattern Recognition (CVPR)*, 2022. 5

[62] Seonguk Seo, Yumin Suh, Dongwan Kim, Gecho Kim, Jongwoo Han, and Bohyung Han. Learning to Optimize Domain Specific Normalization for Domain Generalization. In *Proceedings of the European Conference on Computer Vision (ECCV)*, 2020. 2

[63] Jaehyeok Shim, Changwoo Kang, and Kyungdon Joo. Diffusion-Based Signed Distance Fields for 3D Shape Generation. In *Proceedings of the IEEE/CVF Conference on Computer Vision and Pattern Recognition (CVPR)*, 2023. 5

[64] Xingyuan Sun, Jiajun Wu, Xiuming Zhang, Zhoutong Zhang, Chengkai Zhang, Tianfan Xue, Joshua B. Tenenbaum, and William T. Freeman. Pix3D: Dataset and Methods for Single-Image 3D Shape Modeling. In *Proceedings of the IEEE/CVF Conference on Computer Vision and Pattern Recognition (CVPR)*, 2018. 1, 2, 6, 7, 8

[65] Jiaxiang Tang, Zhaoxi Chen, Xiaokang Chen, Tengfei Wang, Gang Zeng, and Ziwei Liu. LGM: Large Multi-View Gaussian Model for High-Resolution 3D Content Creation. In *Proceedings of the European Conference on Computer Vision (ECCV)*, 2024. 1, 2, 3, 8

[66] Josh Tobin, Rachel Fong, Alex Ray, Jonas Schneider, Wojciech Zaremba, and Pieter Abbeel. Domain Randomization for Transferring Deep Neural Networks from Simulation to the Real World. In *IEEE/RSJ International Conference on Intelligent Robots and Systems (IROS)*, 2017. 2

[67] Dmitry Tochilkin, David Pankratz, Zexiang Liu, Zixuan Huang, Adam Letts, Yangguang Li, Ding Liang, Christian Laforet, Varun Jampani, and Yan-Pei Cao. TripoSR: Fast 3D Object Reconstruction from a Single Image. *arXiv preprint arXiv:2403.02151*, 2024. 1, 2, 3, 8

[68] Jonathan Tremblay, Aayush Prakash, David Acuna, Mark Brophy, Varun Jampani, Cem Anil, Thang To, Eric Cameracci, Shaad Boochoon, and Stan Birchfield. Training Deep Networks With Synthetic Data: Bridging the Reality Gap by Domain Randomization. In *IEEE Conference on Computer Vision and Pattern Recognition (CVPR) Workshops*, 2018. 2

[69] Shubham Tulsiani, Tinghui Zhou, Alexei A Efros, and Jitendra Malik. Multi-view supervision for single-view reconstruction via differentiable ray consistency. In *Proceedings of the IEEE Conference on Computer Vision and Pattern Recognition (CVPR)*, 2017. 2

[70] Ashish Vaswani, Noam Shazeer, Niki Parmar, Jakob Uszkoreit, Llion Jones, Aidan N Gomez, Łukasz Kaiser, and Illia Polosukhin. Attention is All you Need. In *Advances in Neural Information Processing Systems (NIPS)*, 2017. 3

[71] Hemanth Venkateswara, Jose Eusebio, Shayok Chakraborty, and Sethuraman Panchanathan. Deep Hashing Network for Unsupervised Domain Adaptation. In *Proceedings of the IEEE Conference on Computer Vision and Pattern Recognition (CVPR)*, 2017. 2, 6, 7, 8

[72] Nanyang Wang, Yinda Zhang, Zhuwen Li, Yanwei Fu, Wei Liu, and Yu-Gang Jiang. Pixel2Mesh: Generating 3D Mesh Models from Single RGB Images. In *Proceedings of the European Conference on Computer Vision (ECCV)*, 2018. 2

[73] Zhengyi Wang, Yikai Wang, Yifei Chen, Chendong Xiang, Shuo Chen, Dajiang Yu, Chongxuan Li, Hang Su, and Jun Zhu. CRM: Single Image to 3D Textured Mesh with Convolutional Reconstruction Model. In *Proceedings of the European Conference on Computer Vision (ECCV)*, 2024. 1, 2, 3, 8

[74] Chao-Yuan Wu, Justin Johnson, Jitendra Malik, Christoph Feichtenhofer, and Georgia Gkioxari. Multiview Compressive Coding for 3D Reconstruction. In *Proceedings of the IEEE/CVF Conference on Computer Vision and Pattern Recognition (CVPR)*, 2023. 3, 4

[75] Jiajun Wu, Yifan Wang, Tianfan Xue, Xingyuan Sun, William T Freeman, and Joshua B Tenenbaum. MarrNet: 3D Shape Reconstruction via 2.5D Sketches. In *Advances in Neural Information Processing Systems (NIPS)*, 2017. 2

[76] Jiajun Wu, Chengkai Zhang, Tianfan Xue, William T. Freeman, and Joshua B. Tenenbaum. Learning a Probabilistic Latent Space of Object Shapes via 3D Generative-Adversarial Modeling. In *Advances in Neural Information Processing Systems (NIPS)*, 2017. 5

[77] Jiajun Wu, Chengkai Zhang, Xiuming Zhang, Zhoutong Zhang, William T. Freeman, and Joshua B. Tenenbaum. Learning Shape Priors for Single-View 3D Completion and Reconstruction. In *Proceedings of the European Conference on Computer Vision (ECCV)*, 2018. 2

[78] Jianxiong Xiao, James Hays, Krista A. Ehinger, Aude Oliva, and Antonio Torralba. SUN database: Large-scale scene recognition from abbey to zoo. In *Proceedings of the IEEE Conference on Computer Vision and Pattern Recognition (CVPR)*, 2010. 6

[79] Jiale Xu, Weihao Cheng, Yiming Gao, Xintao Wang, Shenghua Gao, and Ying Shan. InstantMesh: Efficient 3D Mesh Generation from a Single Image with Sparse-view Large Reconstruction Models. *arXiv preprint arXiv:2404.07191*, 2024. 2

[80] Lihe Yang, Bingyi Kang, Zilong Huang, Zhen Zhao, Xiaogang Xu, Jia Shi Feng, and Hengshuang Zhao. Depth Anything V2. In *Advances in Neural Information Processing Systems (NeurIPS)*, 2024. 5, 7

[81] Xiangyu Yue, Yang Zhang, Sicheng Zhao, Alberto Sangiovanni-Vincentelli, Kurt Keutzer, and Boqing Gong. Domain Randomization and Pyramid Consistency: Simulation-to-Real Generalization Without Accessing Target Domain Data. In *Proceedings of the IEEE/CVF International Conference on Computer Vision (ICCV)*, 2019. 2

[82] Cheng Zhang, Zhaopeng Cui, Yinda Zhang, Bing Zeng, Marc Pollefeys, and Shuaicheng Liu. Holistic 3D Scene Understanding from a Single Image with Implicit Representation. In *Proceedings of the IEEE/CVF Conference on Computer Vision and Pattern Recognition (CVPR)*, 2021. 2, 6

[83] Lvmin Zhang, Anyi Rao, and Maneesh Agrawala. Adding Conditional Control to Text-to-Image Diffusion Models. In *Proceedings of the IEEE/CVF International Conference on Computer Vision (ICCV)*, 2023. 1, 3, 5, 6

[84] Mengqi Zhang, Yang Fu, Zheng Ding, Sifei Liu, Zhuowen Tu, and Xiaolong Wang. HOIDiffusion: Generating Realistic 3D Hand-Object Interaction Data. In *Proceedings of the IEEE/CVF Conference on Computer Vision and Pattern Recognition (CVPR)*, 2024. 3

[85] Xiuming Zhang, Zhoutong Zhang, Chengkai Zhang, Joshua B. Tenenbaum, William T. Freeman, and Jiajun Wu. Learning to Reconstruct Shapes from Unseen Classes. In *Advances in Neural Information Processing Systems (NeurIPS)*, 2018. 2

[86] Bolei Zhou, Agata Lapedriza, Aditya Khosla, Aude Oliva, and Antonio Torralba. Places: A 10 Million Image Database for Scene Recognition. In *IEEE Transactions on Pattern Analysis and Machine Intelligence (TPAMI)*, 2018. 6

[87] Kaiyang Zhou, Yongxin Yang, Timothy Hospedales, and Tao Xiang. Learning to Generate Novel Domains for Domain Generalization. In *Proceedings of the European Conference on Computer Vision (ECCV)*, 2020. 2

[88] Kaiyang Zhou, Yongxin Yang, Yu Qiao, and Tao Xiang. Domain Generalization with MixStyle. In *International Conference on Learning Representations (ICLR)*, 2021. 2